The Kasian volcanic rocks, Khorramabad, Iran: Evidence for a Jurassic Intra-Oceanic island arc in Neo-Tethys ocean

A. Zarasvandi[1], M. Rezaei[1]*, D. Lentz[2], H. Pourkaseb[1] and M. Karevani[2]

[1]Department of Geology, Faculty of Earth Science, Shahid Chamran University (SCU), Ahvaz, Iran
[2]Department of Earth Sciences, University of New Brunswick, New Brunswick, Canada
E-mail: mn-rezaei@phdstu.scu.ac.ir

Abstract

The Kasian volcanic body is located in the eastern margin of the Zagros thrust belt, close to the Sanandaj-Sirjan metamorphic zone. These volcanic rocks are mainly composed of andesite and andesite-basalt rocks with porphyritic, hypocrystalline porphyritic, hyalo-porphyritic and hyalo-microlitic porphyritic textures. Analyses of the distributions of major, rare earth and trace elements reveal a tholeiitic nature and evidence such as enrichment of Pb and LILE (e.g., U, Rb, Ba), depletion in HFSE (e.g., Nb, Ti, Y), slight enrichment of LREE relative to HREE and trace elements discrimination plots reveal island arc affinity for the Kasian volcanic rocks. Some characteristics like, low Nd/Pb and Ce/Pb values (average 8.76 and 12.70, respectively), high U values and low Nb/U ratios (average 3.52) indicate enrichment of mantle wedge by contribution of slab-derived fluids during dehydration of subducting slab of Neo-Tethys oceanic lithosphere. Moreover, the results show these volcanic rocks to have fractionated as they ascended to higher crustal levels. The results of this study are consistent with the new tectonic scenario for the Sanandaj-Sirjan zone, which suggests that during ocean–ocean subduction (from Jurassic to Cretaceous) an immature island arc developed before the closure of Neo-Tethys ocean.

Keywords: Geochemistry; Zagros orogeny; Kasian; Intra oceanic island arc; Iran

1. Introduction

The geotectonic evolution of the Zagros orogenic and metallogenic belt, a part of Tethyan region has been investigated in many of publications. According to Alavi (2004), the formation of the Zagros orogenic belt can be summarized into three major consecutive events consisting of: (1) subduction of Neo-Tethys ocean floor beneath the Central Iranian Micro-continent, (2) obduction of allochthonous fragments of Neo-Tethys oceanic crust over the Afro-Arabian passive continental margin, and finally (3) continental collision between the Iranian plates and Afro-Arabian continental margin that was followed by closure of Neo-Tethys during the Tertiary. These sequential geotectonic events formed the major tectonic elements with NW-SE trend in western Iran; they consist of the Zagros Fold and Thrust belt (ZFTB), the Sanandaj-Sirjan metamorphic Zone (can be subdivided into north SSZ and south SSZ), and the Urumieh-Dokhtar Magmatic Arc (UDMA; Fig. 1) (Mohajjel et al., 2003; Alavi, 2007). The complex geological history of SSZ has been regarded as one of the most striking features of Zagros orogeny and

several attempts have been made to provide a comprehensive overview on the geotectonic evolution of SSZ (Mohajjel et al., 2003; Ghasemi and Talbot, 2006). The Kasian volcanic body is located in the eastern margin of the Zagros Thrust Belt and in the vicinity of north SSZ. There are widespread occurrences of arc-related plutonic and plutono-metamorphic complexes (e.g., Alvand, Almogholagh, Aligoodarz, Samen, Ghorveh, Borojerd, Urumieh, Arak, Astaneh, Qori, and Siah-Kuh) and volcanic and volcaniclastic rocks (e.g., Hassanabad unit in the Neyriz ophiolite, volcanic rocks of Kermanshah ophiolites, SCV: Cretaceous volcanic rocks in the northwest Iran) along the SSZ (Babaie et al., 2001; Azizi and Jahangiri, 2008; Shahbazi et al., 2010; Esna-Ashari et al., 2012). The SSZ and above plutono-metamorphic complexes have been the subject of numerous petrological, geochronological, geochemical, and structural studies (Baharifar et al., 2004; Ahmadi Khalaji et al., 2007; Azizi and Jahangiri, 2008; Sarkarinejad et al., 2008; Ghalamghash et al., 2009; Rajaieh et al., 2010; Shahbazi et al., 2010; Esna-Ashari et al., 2012). The available data on the volcanic rocks of SSZ is mainly restricted to ophiolitic successions and small-scale volcanic sequences, such as the Kasian volcanic body have not yet been studied. The present study concentrates

---

on geochemical characteristics of the Kasian volcanic rocks as a tool for geodynamic interpretation and metallogenic analysis.
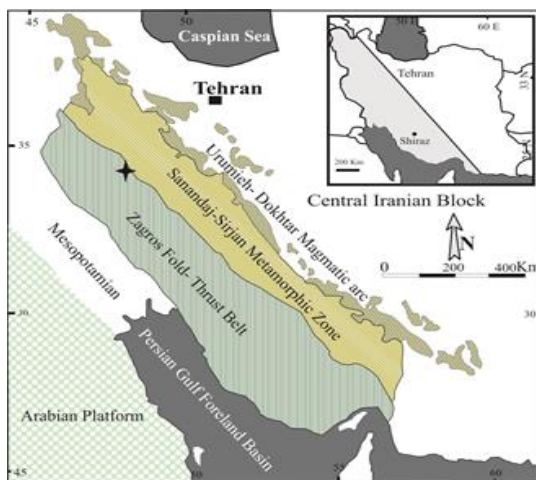
Fig. 1. Geological map Zagros orogenic belt. Modified from Alavi (2004)

2. Geological Framework

The Kasian volcanics are located 70 km northeast of Khorramabad city between 33º38′ -33º42′N and 48º35′-48º39′E. They form a NW–SE-trending body, situated along the eastern edge of Zagros thrust belt and in the vicinity of Sanandaj-Sirjan metamorphic zone (Fig. 2). Detailed interpretations of geological aspects of the study area are scarce and mainly restricted to unpublished reconnaissance reports.

Structurally, this region can be subdivided into three parts: (1) The metamorphic zone that is exposed in the north and northeast part of the study area and mainly includes metavolcanic rocks, marble, slate, and sandy tuff. The Middle Jurassic Boroujerd Granitoid Complex can be divided into three major rock units, namely granodioritic unit, quartz dioritic unit and monzogranitic unit was emplaced in this zone (Ahmadi Khalaji et al., 2007); (2) Autochthon zone that is mainly dominated by NW–SE-trending Mesozoic and Cenozoic sedimentary successions; (3) Allochthon zone consist of Chaghalvandi and Garrin units (Hajmollaali et al., 1991). The Garrin unit consisting of Jurassic-Cretaceous limestone is evident in the northern part of study area. The Chaghalvandi unit consists of limestone, marl, limestone-marl and upper Cretaceous Alveolina limestone overlay the Jurassic Kasian volcanic body (Fig. 3); this unit was thrust over the Miocene sedimentary rocks (Fig. 2).

The Kasian volcanic rocks cover an area of 22.52 km^2 which is composed of andesite and andesite-basalt rocks. Mineral constituents of andesite and andesite-basalt rocks are mainly plagioclase, pyroxene, and K-feldspar with calcite, chlorite and sericite common secondary minerals. Anhedral grains of pyrite also occur locally in the groundmass. Some textures such as porphyritic, hypocrystalline porphyritic,
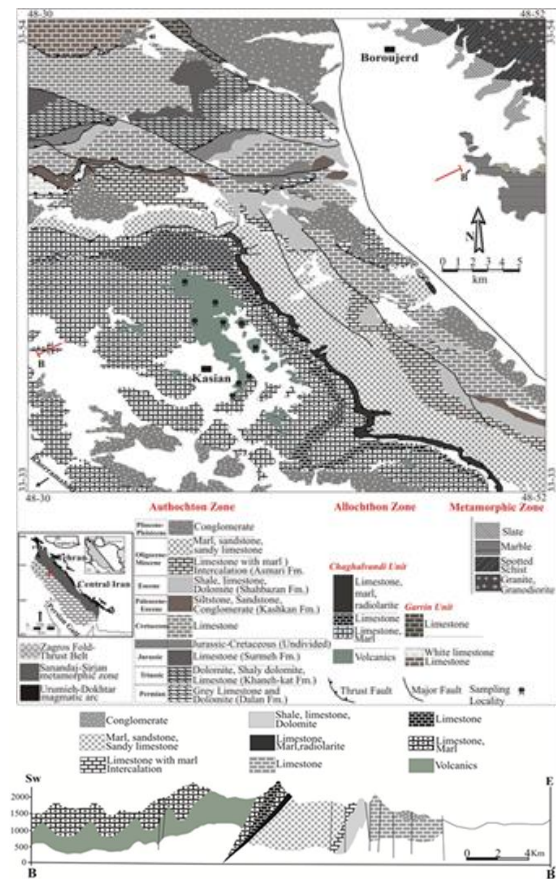
Fig. 2. Local Geological map of the study area with sampling shown within the Jurassic Kasian volcanic sequence and B-B′ geological cross section (modified from Hajmollaali et al. 1991)

Fig. 3. Field photographs of Kasian volcanic rocks, overlying Cretaceous limestones. Photo is looking northwest

Hyalo-porphyritic, and hyalo-microlitic porphyritic are frequent in the rock samples. Plagioclase is the most abundant phenocryst and commonly exhibits sieve, glomeroporphyritic, embayments, and well defined zoning textures. Plagioclase also occurs as fine grained (0.1-0.2 mm) and extended euhedral to subhedral stout prisms (0.5-5 mm), which are either fresh or sericitized and kaolinitized. Plagioclase in the fine-grained groundmass occurs as microlites and laths, occasionally forming pilotaxitic texture. They are generally dusted due to sericitization, with minor calcite. Pyroxene occurs as the main ferromagnesian phenocryst. Phenocrysts of pyroxene are moderately fractured and partially to completely replaced by chlorite. Ferromagnesians are occasionally present as microphenocrysts, which are completely altered to chlorite. In some samples intergrowth between the pyroxene and plagioclase crystals is observed, as well as embayment textures along the rims of pyroxene phenocrysts, representing the instability of these pyroxenes during ascent through the crust (Azizi and Jahangiri, 2008).

3. Methodology

Samples of the andesite and andesite-basalt rocks were collected from the Kasian volcanic body. Thin sections were made from the chosen 135 rock samples and studied by optical microscope. For the petrochemical analysis, 9 least-altered and fractured samples were chosen and then crushed using an iron pestle and were subsequently pulverized using a tungsten carbide swing mill. Concentrations of major, trace, and rare earth elements (REEs) were obtained by lithium metaborate fusion with nitric digestion followed by inductively coupled plasma-mass spectrometry (ICP-MS) and ICP-emission spectrometry (ICP-ES) at ACME Analytical Laboratories, Vancouver, Canada. For the major elements, the detection limit is between 0.002 and 0.01 wt.%, 0.02–2 ppm for the trace elements, and 0.1–0.01 ppm for the REE elements. The analytical results for the major and trace elements of the samples are given in Table 1 and their sample locations shown in Fig. 2.

Table 1a. Content of major oxides (wt %) and trace elements (ppm) in rocks of the Kasian

Sample	AK1A	AK1B	AK2A	AK2B	AK3	AK4	3CH	4MD-6	5EK-7
SiO_2	50.57	61.00	53.42	67.91	60.08	61.77	52.26	55.16	43.42
Al_2O_3	16.16	15.71	15.95	15.49	14.90	14.63	16.33	16.04	16.34
Fe_2O_{3T}	8.18	10.24	7.80	4.58	6.23	5.29	7.33	6.96	8.57
MgO	4.42	1.69	2.09	0.48	2.02	2.02	3.39	2.63	2.44
CaO	6.68	0.85	7.08	1.07	10.86	7.69	6.20	5.91	19.12
Na_2O	4.25	5.16	5.54	8.35	1.51	3.17	6.32	3.81	1.53
K_2O	0.82	0.65	0.58	0.36	0.05	0.41	0.14	0.55	0.02
TiO_2	0.51	0.47	0.53	0.66	0.47	0.54	0.47	0.56	1.05
P_2O_5	0.10	0.11	0.10	0.16	0.10	0.10	0.06	0.15	0.14
MnO	0.16	0.11	0.16	0.03	0.12	0.10	0.11	0.13	0.12
Cr_2O_3	0.025	0.022	0.010	0.051	0.008	0.040	0.041	0.003	0.037
LOI	8.0	3.9	6.6	0.8	3.5	4.1	7.2	8.0	7.0
SUM	99.87	99.91	99.86	99.94	99.84	99.86	99.85	99.90	99.87
Cs	0.3	0.1	0.1	0.02	0.0	0.1	0.1	0.3	0.0
Rb	2.4	2.3	1.8	0.2	0.3	0.9	0.3	1.6	0.3
Ba	10.8	8.4	9.8	13.9	5.3	15.0	9.3	170.7	2.0
Sr	14.8	6.2	18.5	7.8	41.8	13.7	15.8	94.1	198.6
Hf	0.14	0.11	0.20	0.70	0.18	0.15	0.08	0.02	0.27
Ta	0.1	0.1	0.1	0.9	0.1	0.1	0.1	0.3	0.2
Pb	0.5	4.8	2.3	1.5	0.8	0.4	0.6	1.6	1.4
Nb	1.4	1.0	1.7	14.7	1.0	1.4	1.0	3.7	2.7
Th	0.2	0.2	0.2	1.5	0.3	0.2	0.2	0.6	0.1
Co	19.1	17.7	15.1	3.5	13.4	10.6	19.1	12.1	25.3

Ni	8.5	23.3	7.5	5.4	8.4	9.1	10.7	3.7	72.5
V	191	161	208	34	183	174	194	113	212
As	5.9	40	8.6	5.9	5.1	2.1	5.3	2.1	2.3
Cu	5	51	113	19	8	59	8	24	10
Mo	0.09	0.57	0.08	0.49	0.13	0.13	0.11	0.04	0.18
Zn	61.6	60.1	57.8	36.0	39.9	67.2	65.9	71.9	37.9
U	1.0	0.3	1.0	2.0	0.9	0.8	0.2	0.4	2.0
Sc	12.0	9.5	14.9	3.2	10.3	12.8	20.6	7.8	6.4
Zr	32.7	29.3	31.1	509.8	35.9	31.0	32.3	58.4	85.8
Y	9.41	5.47	7.23	21.44	7.02	7.05	7.41	5.74	10.83
Na_2O/K_2O	5.18	7.93	9.55	23.19	30.20	7.73	45.14	6.92	76.50
Ce/Pb	13.80	1.37	4.04	41.66	8.75	16.25	9.33	9.81	9.28
Nd/Pb	11.80	0.87	2.60	24	7.37	14	6.33	4.93	7
Nb/U	1.40	3.33	1.70	7.35	1.11	1.75	5.00	9.25	1.35
Th/Nb	0.28	0.70	0.35	0.44	0.70	0.42	0.70	0.54	0.03

Table 1b. REEs concentration (ppm) in the Kasian volcanic body

Sample	AK1A	AK1B	AK2A	AK2B	AK3	AK4	3CH	4MD-6	5EK-7
La	2.6	2.4	3.8	24.6	3.1	2.6	2.4	7.0	4.3
Ce	6.9	6.6	9.3	62.5	7.0	6.5	5.6	15.7	13.0
Pr	1.09	0.93	1.1	7.98	1.04	0.9	0.86	1.9	1.87
Nd	5.9	4.2	6.0	36	5.9	5.6	3.8	7.9	9.8
Sm	1.70	1.20	1.50	7.64	1.49	1.35	1.23	1.96	2.82
Eu	0.59	0.47	0.59	1.80	0.50	0.53	0.53	0.78	1.05
Gd	2.34	1.64	1.78	8.30	2.02	1.89	1.83	2.73	3.60
Tb	0.44	0.33	0.32	1.48	0.39	0.35	0.33	0.44	0.65
Dy	2.81	1.89	2.07	9.10	2.40	2.20	2.20	2.63	3.82
Ho	0.60	0.40	0.44	1.93	0.56	0.46	0.42	0.58	0.87
Er	2.10	1.32	1.40	6.76	1.80	1.60	1.52	1.99	2.73
Tm	0.30	0.18	0.20	0.99	0.27	0.23	0.21	0.31	0.41
Yb	1.94	1.31	1.34	6.85	1.74	1.45	1.39	2.06	2.52
Lu	0.31	0.21	0.20	1.05	0.27	0.22	0.23	0.32	0.38
$\sum$REE	29.62	23.08	30.04	176.98	28.48	25.88	22.55	46.3	47.82
LREE/HREE	1.73	2.17	2.87	3.85	2.01	2.08	1.77	3.18	2.19
Eu/Eu*	0.90	1.02	1.10	0.69	0.88	1.01	1.08	1.03	1.00
Gd_N/Yb_N	0.97	1.01	1.07	0.97	0.93	1.05	1.06	1.07	1.15
La_N/Sm_N	0.96	1.25	1.59	2.02	1.30	1.21	1.22	2.24	0.96
Ce_N/Yb_N	0.92	1.30	1.79	2.36	1.04	1.16	1.04	1.97	1.33

4. Geochemistry

4.1. Assessment of element mobility due to alteration

In spite of precautions in careful selection of samples, a relatively high loss on ignition (LOI) in the samples (average, 5.45 wt.%) attests to a variable degree of alteration of the rock samples. Previous studies on elemental mobility during the alteration and regional metamorphism have demonstrated that different elements display different degrees of mobility (Winchester and Floyd, 1976; Polat and Hofmann, 2003). Many of the major and trace elements (e.g., Si, Na, K, Ca, Cs, Rb, Ba, Sr) are easily mobilised during post-magmatic processes; however, the HFSEs (e.g., Th, Ti, Zr, Nb), REEs and transition elements (V, Cr, Ni and Sc), are considered as being relatively immobile during low grade metamorphism or alteration processes (Bédard, 1999). According to Maurice et al. (2012) correlation diagrams between the immobile and elements indicator of differentiation (e.g., Zr) can be used in identifying the mobility of elements during alteration and regional metamorphism. There are good linear correlations between REEs and HFSE (Fig. 4), suggesting that the ratios between these elements remain constant and provide evidence that geochemical arrangement of these elements was probably not substantially modified by the post-eruptive low temperature alteration processes.
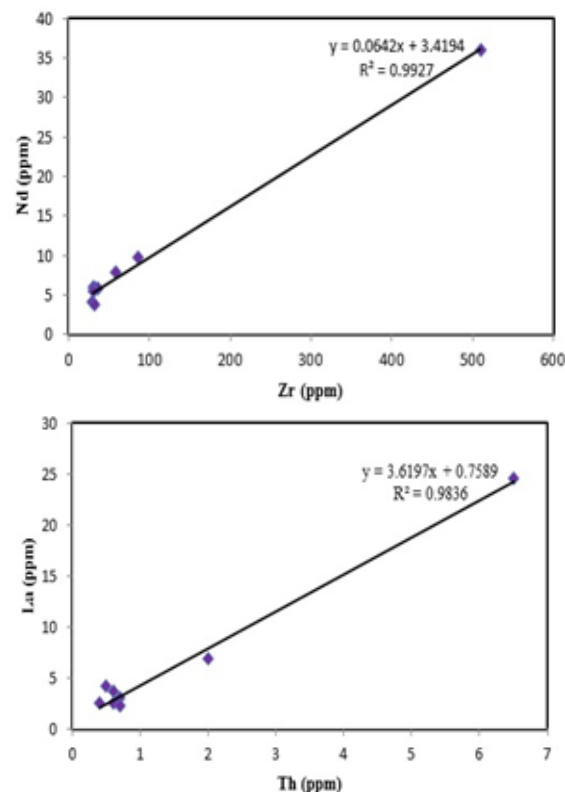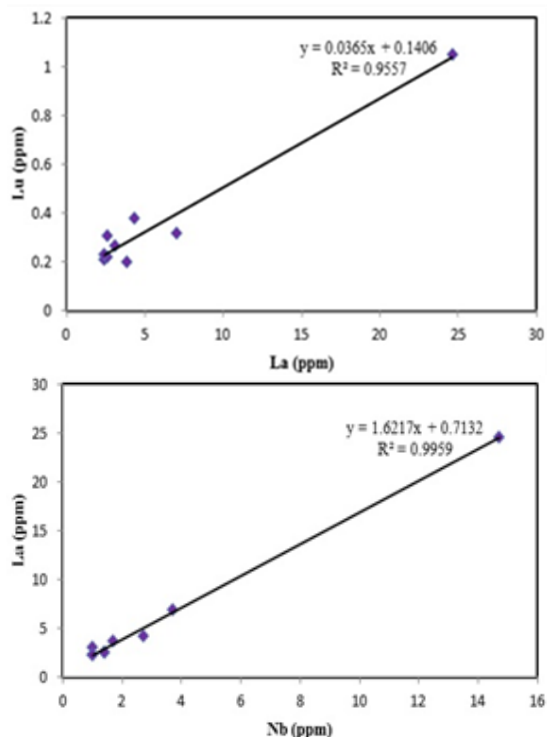
Fig. 4. Examples of good linear correlation between the LREE, HREE and HFSE

Therefore, the subsequent petrogenetic and geochemical interpretations, as well as tectonic setting discrimination of Kasian samples are mostly based on immobile HFSE and REEs, which have similar chemical and physical properties to each other.

4.2. Major Oxides

A summary of the major oxides of Kasian volcanic rocks is provided in Table 1a. The rocks have SiO_2 values between 43.42- 67.91wt.% with MgO of 0.48-4.42 wt.% and Fe_2O_3 of 4.58-10.24 wt.%. The K_2O concentration is between 0.02-0.82 wt.% and Na_2O between 1.51-8.35 wt.%. The samples contain 14.63-16.34 wt.% Al_2O_3 with 0.47-1.05 wt.% TiO_2 contents. In the Zr/TiO_2 versus Nb/Y compositional discrimination diagram (Winchester and Floyd 1977), with the exception of two samples, all selected samples are plotted in the andesite-basalt field (Fig. 5).
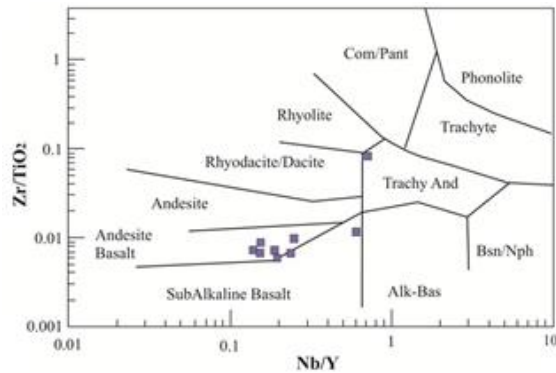
Fig. 5. Zr/TiO2 versus Nb/Y plot (Winchester and Floyd 1977) for the compositional classification of the volcanic rocks of Kasian area

Using SiO2 as a fractionation index, MgO, Fe2O3, MnO, Al2O3, and CaO contents represent negative correlation with SiO2 content, whereas Na2O content display positive correlation and TiO2, P2O5, K2O and Cr2O3 are scattered and exhibit no consistent relationship with SiO2 content (Fig. 6). The negative correlation between SiO2 and some major oxides (e.g., MgO, Fe2O3, CaO, Al2O3, and MnO) suggest that these volcanic rocks experienced fractionation.

The samples have total alkali (Na2O+K2O) contents ranging from 1.55 to 8.71 wt.% and display a wide range of Na2O/K2O ratio from 5.18 to 76.5 (average 23.59), which can be due to their sodium-rich compositions (Tang et al., 2010). Moreover, the relatively high Na2O values (1.51-8.35 wt.%) and subsequently elevated Na2O/K2O ratios in some samples may be the result of alteration through sub-ocean floor processes (Bonev and Stampfli, 2008). The AFM (Na2O+K2O–FeO^{tot}-MgO; Fig. 7a), K2O versus SiO2 diagram (not shown) and Y versus Zr (Fig. 7b) indicate that almost all of the samples from the Kasian volcanic body belong to the tholeiitic series. Overall, both the discrimination diagrams based on major oxides (Fig. 7a) and immobile HFSE (Fig. 7b) agree well with each other.

4.3 Trace elements

The results of geochemical analyses for trace and rare earth elements (REEs) are listed in Tables 1a-b. On the primitive-mantle-normalized multi-element spider diagram (McDonough and Sun, 1995) the rocks are depleted in High Field Strength Elements (HFSEs; e.g., Nb and Ti) relative to neighboring elements, which may be due to fractionation of a Ti-rich phase at the magma source (Ghalamghash et al., 2009) and with the exception of AK3 and 5EK-7, all samples display enrichment in Large Ion Lithophile Elements (LILEs; e.g., Rb, Ba, U) typical of subduction

zones (Fig. 8). It is important to note that the samples show distinct enrichment and depletion in Pb and Sr values, respectively.
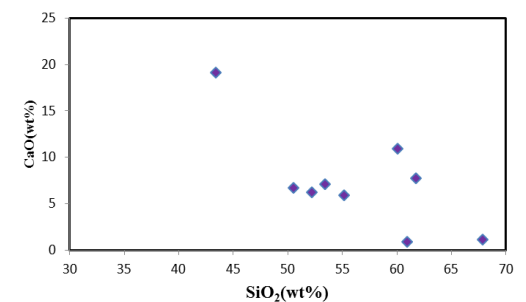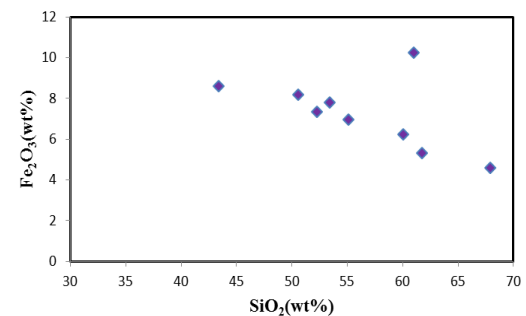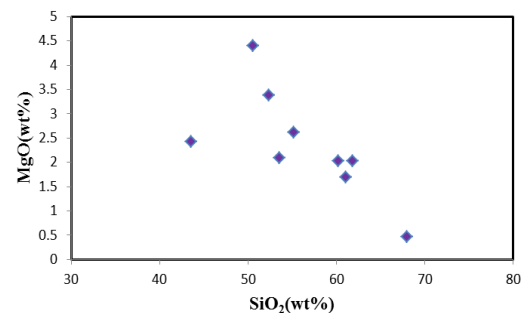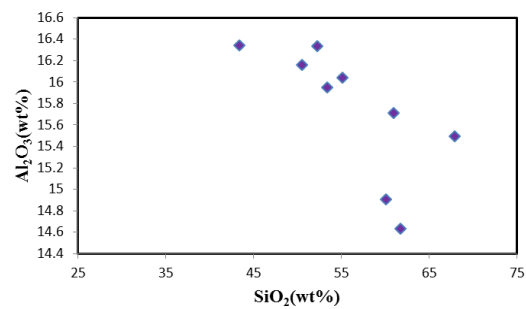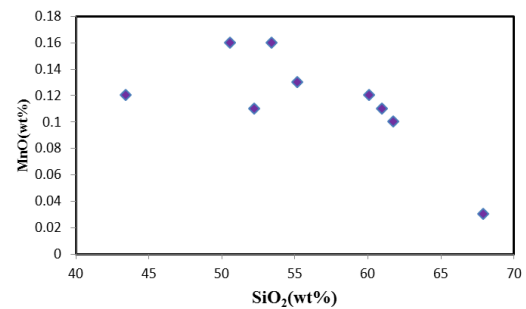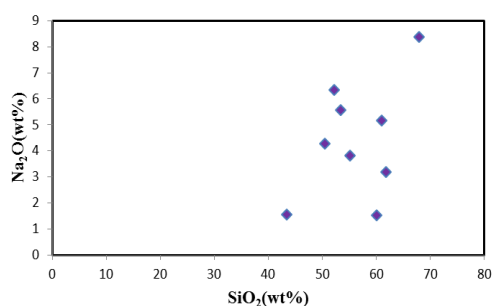
Fig. 6. Major element oxides versus SiO$_2$ plots for the Kasian volcanic rocks

The negative Sr anomaly can be due to fractional crystallization in the magma source. As shown in multi-element spider diagram (Fig. 8), in contrast to HFSEs and REEs no uniformity is observed in LILEs (in the Cs, Rb, and Ba values of the AK3 and 5EK-7), this fact might have resulted from relative mobilities of these elements during post-magmatic processes (Zhang et al., 2008).
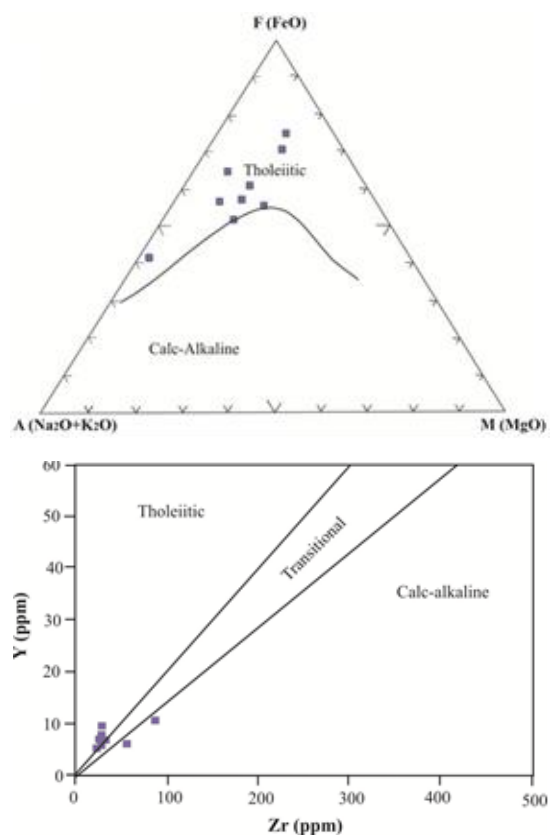
Fig. 7. (a) AFM diagram for Kasian samples. The boundary between tholeiitic and calc-alkaline is from Irvine and Baragar (1971), (b) Zr vs. Y diagram after Barrett and MacLean (1994)

Chondrite-normalized REE patterns of Kasian volcanic rocks are shown in Fig. 9. The La$_N$/Sm$_N$ values range from 0.96 to 2.02 (average 1.43),

which represent a slight enrichment of LREE relative to MREE. The Gd$_N$/Yb$_N$ ratios vary between 0.93 and 1.15 (average 1.05), reflecting flat middle REE (MREE) to Heavy REE (HREE) on the REE patterns normalized relative to chondrite values (Evensen et al., 1978). These features are typical of tholeiitic arc basalts (Chiaradia, 2009). The unfractionated HREE could indicate that magma was produced outside the garnet stability field (Ahmadi Khalaji et al., 2007).

The Eu (Eu/Eu*) anomaly was calculated from: Eu/Eu*=Eu$_n$/(Sm$_n$×Gd$_n$)$^{1/2}$ (Taylor and McLennan, 1985). The Eu anomalies vary between 0.69-1.10 (average 0.97), representing weak negative/or no Eu anomaly for the studied samples. The relatively negative Eu anomalies are consistent with Sr-depletion in the multi-element spider diagram (Fig. 8). It was previously noted that REEs are considered as being relatively immobile during alteration. Plots of studied samples on the La content vs. La/Sm (Zhang et al., 2008) (Fig. 10) indicate that the magmatic evolution could be attributed to the fractional crystallization, which is consistent with the general trend of major oxides on the Harker variation diagrams (Fig. 6). Moreover, according to Wilkinson and Le Maitre (1987) and Frey et al. (1978), rocks with 250–300 ppm Ni, 500–600 ppm Cr and 27 to 80 ppm Co contents are considered to be derived from a primary mantle source. The andesite and andesite-basalt rocks have Ni values ranging
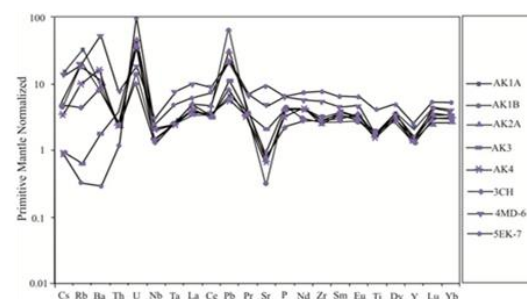
Fig. 8. Primitive mantle-normalized trace-element spider diagram. Normalizing values are from McDonough and Sun (1995)
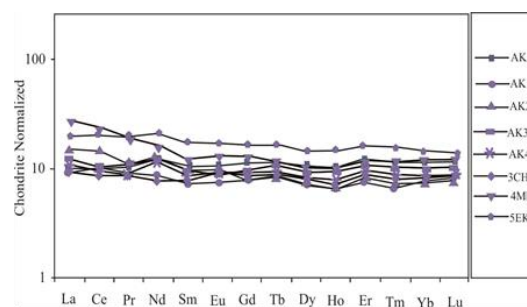
Fig. 9. Chondrite-normalized REE patterns of the Kasian samples, with chondrite values are from Evensen et al. (1978)

From 3.7 to 72.5 ppm, Cr contents from 20 to 340 ppm and Co values varying from 3.5 to 25.3 ppm. These values are lower than those proposed for primary magmas, suggesting that the parent magma for the Kasian that the parent magma for the Kasian rocks had undergone fractionation en-route to eruption (Haq Siddiqui et al., 2012).

5. Discussion

5.1 Arc- related associations

The composition of primitive arc magmas is controlled by partial melting and crystal fractionation of the magma source, which depends on mantle-derived and subducting slab-derived components, during subduction; the incompatible elements (e.g., Rb, Ba, Pb, U, Cs, K, Na) and LREE (e.g., La, Ce) are driven from the subducting slab into the overlying mantle wedge, in contrast HFSEs, including Zr-Hf, Nb-Ta, Ti-V-Sc, and Y are virtually insoluble and immobile during the slab melting processes and therefore their compositions can reflect the composition of mantle wedge (Pearce and Peate, 1995; Viruete et al., 2006). The geochemical characteristics of Kasian volcanic rocks indicate LILE and water enrichment of the mantle wedge (suprasubduction zone) by slab-derived fluids (or melts) during the dehydration of subducting slab of Neo-Tethys oceanic lithosphere; most samples are characterized by relatively low Nd/Pb and Ce/Pb values (average 8.76 and 12.70, respectively); these values are much lower than that of typical MORB (depleted) mantle or ocean island basalts (Nd/Pb=24, Class et al., 2000); (Ce/Pb=27, Hofmann et al., 1986). Such low Ce/Pb ratios likely resulted from source enrichment by slab-derived fluids (Bonev and Stampfli, 2008; Park et al., 2010). The M/Yb vs. Nb/Yb diagrams (Pearce and Peate, 1995) have been widely used in previous studies to evaluate the contribution of mantle and slab-derived components (Manikyamba et al., 2004; Viruete et al., 2006, 2010; Azizi and Jahangiri, 2010; Maurice et al., 2012); here the M refers to conservative (i.e., HFSE) or nonconservative (i.e., LILE or LREE) elements of interest. In the U/Yb versus Nb/Yb plot (Fig. 11a); samples of Kasian are collectively plotted above the MORB-OIB array, indicating the contributions of Uranium from the subduction components. In order to estimate the addition of La (as an example of a nonconservative element) from the subduction components to a mantle source of constant composition, the parallel contour lines have been drawn above the MORB array (Fig. 11b), this diagram shows that the subduction-component contributions for La is approximately up to 50% .
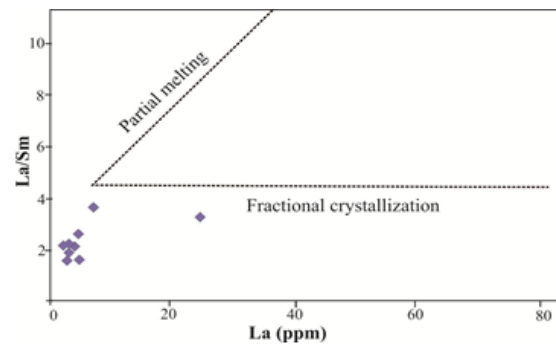
Fig. 10. Plot of andesite and andesite basalt rocks from Kasian on the La vs. La/Sm diagram. Modified from Zhang et al. (2008)

The anomalies in some HFSEs (e.g., Nb, Ti, Y; Fig. 8) are different from MORB, OIB, and CFB that display no or insignificant HFSEs anomalies (Sun and McDonough, 1989; Zhang et al., 2008). It was mentioned above that the slab-derived hydrous fluids are not capable of transferring significant amounts of HFSEs.
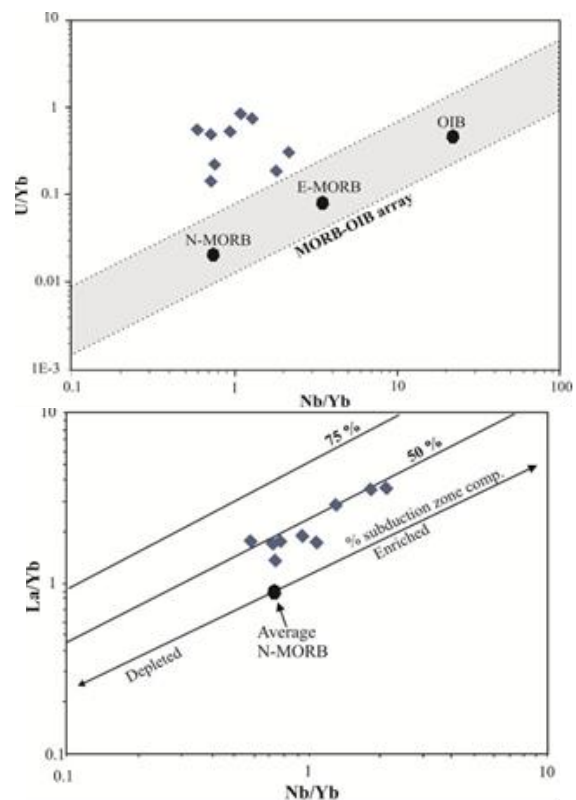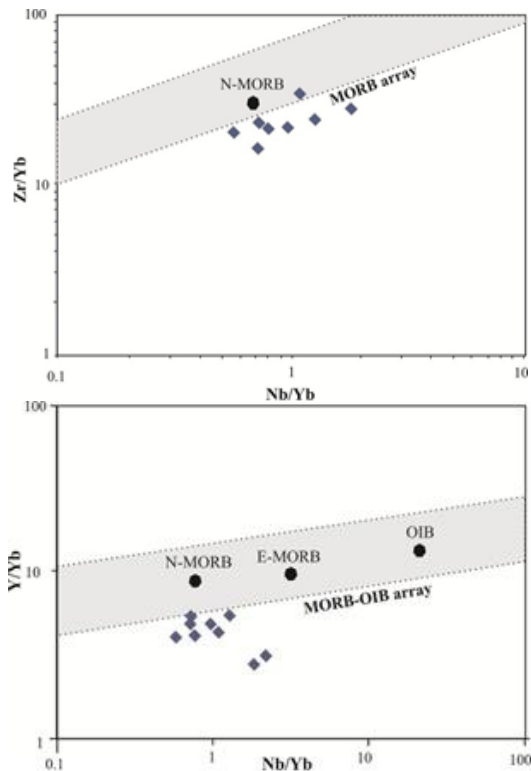
Fig. 11. U/Yb, La/Yb, Zr/Yb and Y/Yb vs. Nb/Y plots for the Kasian rocks. Mantle array in (a) and (e), after Green (2006); mantle array in (b) and (c), after Pearce and Peate (1995). The oriented arrow indicate patterns of enrichment and depletion of an average N-MORB mantle and the solid line (b) shows the amount of subduction zone contribution (Pearce and Peate, 1995)

The contribution of Zr and Y (examples of HFSEs) from the subducting slab of Neo-Tethys oceanic lithosphere is illustrated on the Zr/Yb and Y/Yb vs. Nb/Yb diagrams (Figs. 11c and d), the Kasian samples are collectively plotted near the N-MORB array and below, indicating a mantle origin for approximately all of the Zr and Y contents (Viruete et al., 2010).

It is important to note that the Nb and U have similar solid/melt partition coefficients and consequently mantle melting processes cannot fractionate these elements (Hofmann, 1988; Sun and McDonough, 1989). In the primitive mantle-normalized trace element variation diagram (Fig 8), samples display enrichments in the U relative to adjacent elements (Nb and Th). This feature is consistent with the above interpretations about the contributions of Uranium from the subduction components (see Fig, 11a). The Nb/U values (<10; Table 1b) for the Kasian samples are significantly lower than bulk silicate earth (Nb/U=32), oceanic basalts (Nb/U=50) and upper continental crust (Nb/U=9; Fig. 12a), indicating arc volcanic characteristics for the volcanics under study (Yang et al., 2005; Azizi and Jahangiri, 2008). The arc

characteristic is also supported by plotting of the Kasian samples on the discrimination diagram using immobile HFSE elements (Fig. 12b). In this diagram and many other diagrams (not shown), the Kasian samples fall largely in the arc field.

5.2 Geotectonic discrimination

As mentioned earlier, Kasian samples have relatively high LOI values; such values can highlight the role of alteration during post-eruption processes, the effects of alteration and consequently elemental mobility can be traced on the primitive mantle-normalized multi-element spider diagram (Fig. 8); the concentration of susceptible elements to alteration (e.g., LILs; Rb, Cs and Ba) for some samples are unconformable with the general trend of other samples. However, other parameters, such as mantle metasomatism processes produced by subduction-derived fluids, cannot be ruled out (Zhang et al., 2008).

A variety of tectonomagmatic discrimination plots, based on major and trace elements have been proposed by authors to study the parent magma and tectonic setting of volcanic rocks. It seems that evaluation of Kasian rocks with the use of discrimination plots based on major or LILEs must be done with caution. As mentioned earlier, the HFSEs (e.g., Th, Ti, Zr, Nb) and REEs are considered as being relatively immobile during alteration processes, therefore discrimination plots based on HFSEs and REEs are very useful in discriminating tectonic affinity and origin of eruptive rocks (Yan Wang et al., 2007; Bierlein and Craw, 2009). In the V vs Ti/1000 diagram (Shervais, 1982; not shown), most of the samples occupy the island arc tholeiite field. This is consistent with slight enrichment of LREE relative to HREE (Fig. 9) that is typical of island arc lavas (Chiaradia, 2009; Park et al., 2010).
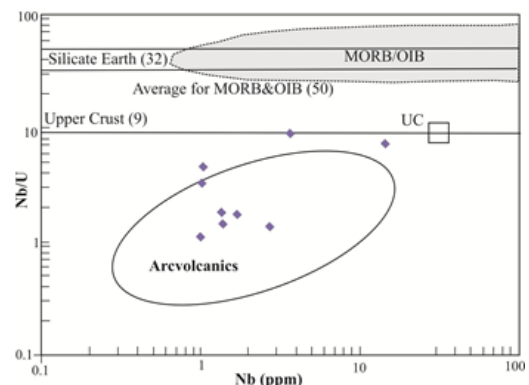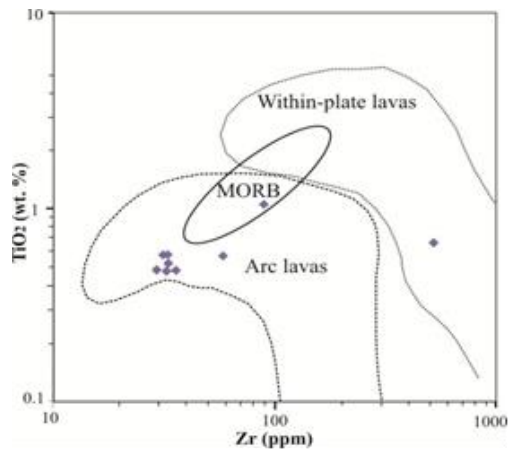
Fig. 12. (a) Nb (ppm) vs Nb/U diagram. Data sources: the values for the MORB/OIB, bulk silicate earth and upper continental crust are from Hofmann et al. (1986), McDonough et al. (1992), McDonough and Sun (1995). The grey shading for MORB/OIB and field of arc volcanics is from (Chung et al. 2001). (b) TiO_2–Zr diagram, after Pearce (1982).

Similarly, the studied rocks fall mainly in the island arc field on the TiO_2 vs Y/Nb diagram (Fig. 13a) of De Albuquerque (1979), La/Yb vs Th/Yb discrimination diagram (Fig. 13b) of Condie (1989) and Th/Yb vs Ta/Yb plot (Fig 13c). The general trend of samples on the Th/Yb vs Ta/Yb diagram (Fig. 13c) indicates fractional crystallization and subduction zone enrichment processes. This feature is also supported by decreases in MgO, Fe_2O_3, MnO, Al_2O_3, and CaO with increasing SiO_2 (Fig. 6), the La vs. La/Sm diagram (Fig. 10) and also the low concentration of Co, Cr and Ni that indicate the parent magma of these rocks was not directly derived from a mantle source but fractionated during ascend to the higher crustal levels. Taken as a whole, petrological and geochemical characteristics confirm a tholeiitic parentage and the oceanic island arc affinity of the Kasian volcanic rocks.
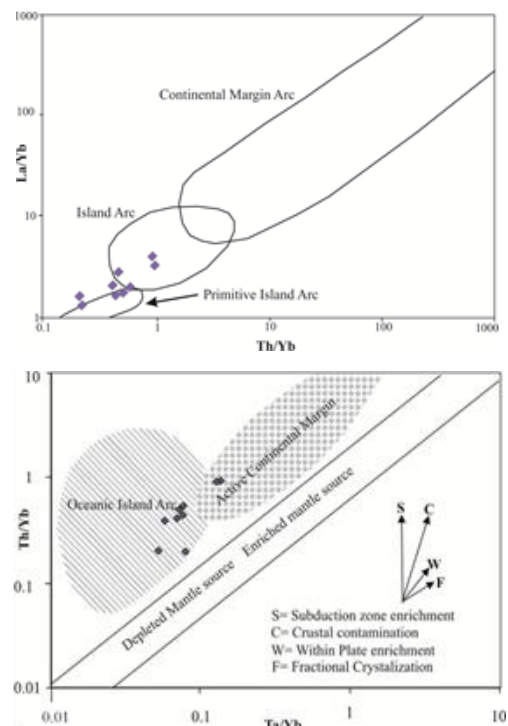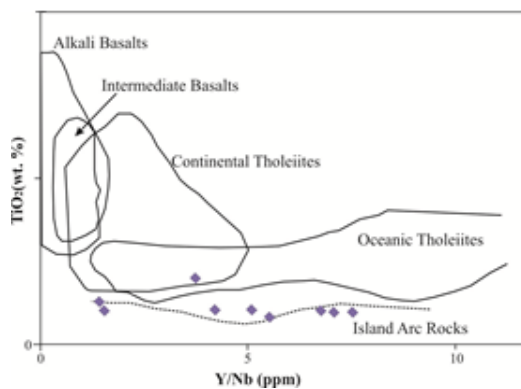
Fig. 13. (a) TiO_2 vs. Y/Nb after De Albuquerque (1979), (b) La/Yb vs. Th/Yb diagram (Condie, 1989) and (c) Th/Yb vs Ta/Yb plot (Pearce, 1983)

Figure 14 represents the comparison of Kasian volcanic rocks with different island arc rocks in the world. The REE patterns of Kasian volcanic rocks are consistent with South Sandwich and New Britain primitive oceanic island arcs (Fig. 14a). The studied samples have relatively low Th and Th/Yb values (0.19-0.97), and are collectively plotted in the field of South Sandwich, Vanuatu, New Britain, Tonga and Mariana island arcs (Fig. 14b). Low Th/Yb values indicate little input of sediments to the melt generated in the mantle wedge (Schuth et al., 2004; Maurice et al., 2012). Another indication of this may be seen in the Zr/Yb vs. Nb/Yb diagram (Fig.11c), where samples are plotted near the N-MORB array and below (because the input of Zr from the melted sediments would result in selective enrichment of Zr and upward displacement from the mantle array).

6. Geodynamic consideration and conclusion

A new tectonic scenario has recently been proposed for SSZ (Ghasemi and Talbot, 2006; Fig. 15). The SSZ was prior to late Paleozoic time, part of stable continental platform in the northeast of Gondwanaland. Some evidence, such as basic (basalt, diabase, and some intermediate) volcanic activity in the north SSZ during Late Permian, Triassic Sikhoran basic-ultrabasic complex in the southern SSZ indicate two rifting phases have been started along the north and south SSZ during Late Permian and middle to late

Triassic time, respectively (Fig. 15a). From Jurassic to Cretaceous time, subduction of Neo-Tethys oceanic crust occurred beneath the SSZ and the SSZ was locally transformed into a magmatic arc geodynamic environment (Fig. 15b). Accordingly, the SSZ was intruded by several granitoid complexes such as Alvand, Almogholagh, Aligoodarz, Samen, Ghorveh, Borojerd, Urumieh, Arak, Astaneh,Qori, and Siahkuh.
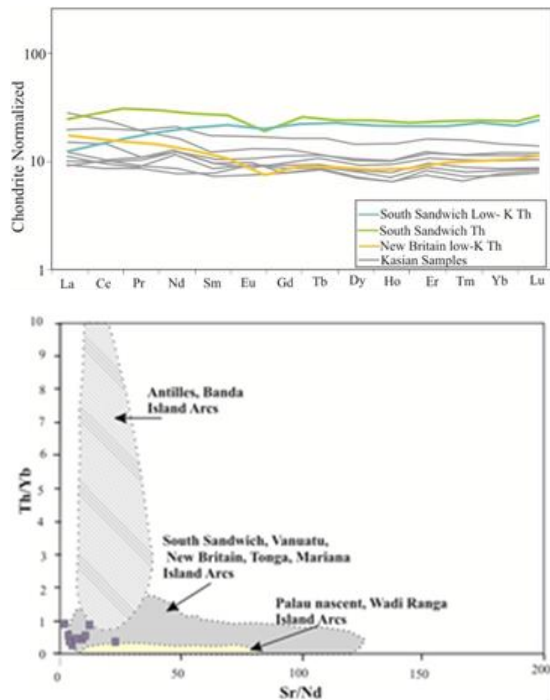
Fig. 14. (a) chondrite-normalized REE patterns of Kasian volcanic rocks compared with other island arc rocks in the world. Chondrite values are from Evensen et al. (1978). The values for the mafic (low-K tholeiitic series) and felsic (low-K tholeiitic and tholeiitic series) rocks of South Sandwich and New Britain are from Leat et al. (2003) and Woodhead et al. (1998), respectively. (b) Comparison of Kasian volcanic rocks with different island arc rocks in the world, with the exception of Wadi Ranga field (Maurice et al., 2012) the fields of different arcs adopted by Hawkins and Ishizuka (2009)

These granitoid complexes generally span in age from Late Triassic to Early Eocene (Arvin et al., 2007; Mazhari et al., 2009). However, the ages and petrogenetic evolution of these rocks have often been questioned. Moreover, geochemical characteristics of volcanic rocks from ophiolite complexes along the Zagros orogeny indicate ophiolitic lavas have geochemical signatures that relate more to subduction zone processes. The available data (mostly about the ophiolite successions) reveal that immature island arc developed before the closure of Neo-Tethys ocean (Babaie et al., 2001). The development of this intra-oceanic island arc was complex (Ghasemi and Talbot, 2006). Moreover, evidence is scarce along the Zagros orogeny. It is thought that intra-oceanic

island arcs were obducted as ophiolites onto the northern margin of Arabian plate in the Late Cretaceous (Fig. 15c) and finally oblique convergence between the Arabian plate and central Iran closed Neo-Tethys in the Early to Middle Eocene (Fig. 15d). The Kasian volcanic body is situated along the eastern edge of the Zagros Thrust belt and in the vicinity of SSZ (Fig. 1). The geological setting together with the geochemical characteristics indicates that volcanics under study could be considered as evidence for intra-oceanic island arcs in Neo-Tethys
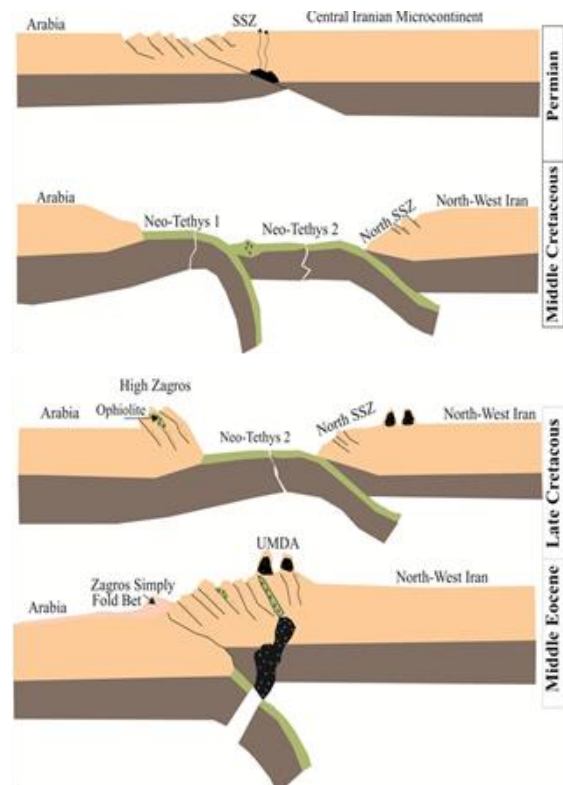
Fig. 15. Tectonic evolution of the north Sanandaj-Sirjan Zone. Modified from Ghasemi and Talbot (2006)

During Jurassic time. The main geochemical characteristics of Kasian volcanics can be summarized as follow:

1- The volcanic rocks represent a low-K tholeiitic suite that underwent minor alteration through sub-ocean floor processes.

2- The depletion in HFSE (e.g., Nb, Ti, Y) and enrichment in LILE (e,g., Rb, Ba, U) indicate involvement of subduction-derived materials in the generation of the Kasian volcanic rocks. Moreover, the trends on Harker diagrams and La vs. La/Sm values with low abundance of Cr, Co and Ni suggest fractional crystallization of the melts during ascent to the higher crustal levels.

3- An enrichment of Pb and relatively low Nd/Pb and Ce/Pb values with slight enrichment of LREE relative to HREE and tectonic discrimination plots

strongly support an island arc tholeiitic signature.

4- The low Zr and Th abundance, with low Th/Yb and Zr/Yb values indicate little sediment input to melt generation in the mantle wedge and provide evidences for the long distance to continental margin. However, more studies, especially radiogenic isotopes (e.g., Nd) are necessary to verify this concept.

References

Ahmadi Khalaji, A., Esmaeily, D., Valizadeh, M. V., & Rahimpour Bonab, H. (2007). Petrology and geochemistry of the granitoid complex of Boroujerd, Sanandaj-Sirjan Zone, western Iran. *Journal of Asian Earth Sciences*, 29, 859–877.

Alavi, M. (2004). Regional stratigraphy of the Zagros fold-thrust belt of Iran and its proforeland evolution. *American Journal of Science*, 304, 1–20.

Alavi, M. (2007). Structures of the Zagros fold-thrust belt in Iran. *American Journal of Science*, 307, 1064–1095.

Arvin, M., Pan, Y., Dargahi, S., Malekizadeh, A., & Babaei, A. (2007). Petrochemistry of the Siah-Kuh granitoid stock southwest of Kerman, Iran: implications for initiation of Neotethys subduction. *Journal of Asian Earth Sciences*, 30, 474–489.

Azizi, H., & Jahangiri, A. (2008). Cretaceous subduction-related volcanism in the northern Sanandaj-Sirjan Zone, Iran. *Journal of Geodynamics*, 45, 178–190.

Babaie, H. A., Ghazi, M. A., Babaie, A., La Tour, T. E., & Hassanipak, A. A. (2001). Geochemistry of arc volcanic rocks of the Zagros Crush Zone, Neyriz Iran. *Journal of Asian Earth Sciences*, 19, 61–76.

Baharifar, A., Moinevaziri, H., Bellon, H., & Piqué, A. (2004). The crystalline complexes of Hamadan (Sanandaj–Sirjan zone, western Iran): metasedimentary Mesozoic sequences affected by Late Cretaceous tectono-metamorphic and plutonic events. *C. R. Geoscience*, 336, 1443–1452.

Barrett, T. J., & MacLean, W. H. (1994). *Chemostratigraphy and hydrothermal alteration in exploration for VHMS deposits in greenstone and younger volcanic rocks*. In D. R. Lentz (Ed.), Alteration and Alteration Processes Associated with Ore-Forming Systems (pp. 433–467). Geological Association of Canada, Short Course Notes, 11.

Bédard, J. H. (1999). Petrogenesis of boninites from the Betts Cove Ophiolite, Newfoundland, Canada: identification of subducted source components. *Journal of Petrology*, 40, 1853–1889.

Bierlein, F. P., & Craw, D. (2009). Petrogenetic character and provenance of metabasalts in the aspiring and Torlesse Terranes, South Island, New Zealand:

Implications for the gold endowment of the Otago Schist?. *Chemical Geology*, 260, 301–315.

Bonev, N., & Stampfli, G. (2008). Petrology, geochemistry and geodynamic implications of Jurassic island arc magmatism as revealed by mafic volcanic rocks in the Mesozoic low-grade sequence, eastern Rhodope, Bulgaria. *Lithos*, 100, 210–233.

Chiaradia, M. (2009). Adakite-like magmas from fractional crystallization and melting-assimilation of mafic lower crust (Eocene Macuchi arc, Western Cordillera, Ecuador). *Chemical Geology*, 265, 468–487.

Chung, S. L., Wang, K. L., Crawford, A. J., Kamenetsk, V. S., Chen, C. H., Lan, C. Y., et al. (2001). High-Mg potassic rocks from Taiwan: implications for the genesis of orogenic potassic lavas. *Lithos*, 59, 153–157.

Class, C., Miller, D. M., Goldstein, S. L., & Langmuir, C. H. (2000). Distinguishing melt and fluid subduction components in Umnak Volcanics, Aleutian arc. *Geochemistry, Geophysics, Geosystems*, doi: 1 1999GC000010.

Condie, K. C., (1989). Geochemical changes in basalts and andesites across the Archean Proterozoic boundary: identification and significance. *Lithos*, 23, 1–18.

De Albuquerque, C. A. R. (1979). Origin of plutonic rocks of southern Nova Scotia. *Geological Society of America Bulletin*, 90, 719–731.

Esna-Ashari, A., Tiepolo, M., Valizadeh, M. V., Hassanzadeh, J., & Sepahi, A. A. (2012). Geochemistry and zircon U–Pb geochronology of Aligoodarz granitoid complex, Sanandaj-Sirjan Zone, Iran. *Journal of Asian Earth Sciences*, 43, 11–22.

Evensen, M. N., Hamilton, P., & O'Nions, R. K. (1978). Rare-earth abundances in 561 chondritic meteorites. *Geochimica et Cosmochimica Acta*, 42, 562–1199.

Frey, F. A., Green, D. H., & Roy, S. D. (1978). Integrated model for basalt petrogenesis: a study of quartz tholeiites to olivine melilite from southeastern Australia, utilizing geochemical and experimental petrological data. *Journal of Petrology*, 19, 463–513.

Ghalamghash, J., Nedelec, A., Bellon, H., Vousoughi Abedini, M., & Bouchez, J. L. (2009). The Urumieh plutonic complex (NW Iran): A record of the geodynamic evolution of the Sanandaj–Sirjan zone during Cretaceous times – Part I: Petrogenesis and K/Ar dating. *Journal of Asian Earth Sciences*, 35, 401–415.

Ghasemi, A., & Talbot, C. J. (2006). A new tectonic scenario for the Sanandaj–Sirjan Zone (Iran). *Journal of Asian Earth Sciences*, 26, 683–693.

Green, N. L. (2006). Influence of slab thermal structure on basalt source regions and melting conditions: REE and HFSE constraints on from the Garibaldi volcanic belt, northern Cascadia subduction system. *Lithos*, 87, 23–49.

Hajmollaali, A., Hosseini, M., Farhadian, M. B., & Sedaghat, E. (1991). Geological quadrangle map of the Boroujerd area, No: D 7.1: 100 000, *Geological Survey of Iran*, Tehran, Iran.

Haq Siddiqui, R., Qasim Jan, M., & Asif Khan, M. (2012). Petrogenesis of Late Cretaceous lava flows from a Ceno-Tethyan island arc: The Raskoh arc,

Balochistan, Pakistan. *Journal of Asian Earth Sciences*, 59, 24–38.

Hawkins, J. W., & Ishizuka, O. (2009). Petrologic evolution of Palau, a nascent island arc. *Island Arc*, 18, 599–641.

Hofmann, A. W. (1988). Chemical differentiation of the earth: the relation between mantle, continental crust and oceanic crust. *Earth and Planetary Science Letters*, 90, 297–314.

Hofmann, A. W., Jochum, K. P., & Seufert, M. (1986). Nb and Pb in oceanic basalts: new constraints on mantle evolution. *Earth and Planetary Science Letters*, 79, 33–45.

Irvine, T. N., & Baragar, W. R. A. (1971). A guide to the chemical classification of the common volcanic rocks. *Canadian Journal of Earth Sciences*, 8, 523–548.

Leat, P. T., Smellie, J. L., Millar, I. L., & Larter, R. D. (2003). *Magmatism in the South Sandwich arc*. In R. D. Larter, & P. T. Leat (Eds.), Intra-Oceanic Subduction Systems: Tectonic and Magmatic Processes (pp. 285–313). Geological Society of London, Special Publication, 219.

Manikyamba, C., Kerrich, R., Naqvi, S. M., & Ram Mohan, M. (2004). Geochemical systematics of tholeiitic basalts from the 2.7 Ga Ramagiri-Hungund composite greenstone belt, Dharwar craton. *Precambrian Research*, 134, 21–39.

Maurice, A. E., Basta, F. F., & Khiamy, A. A. (2012). Neoproterozoic nascent island arc volcanism from the Nubian Shield of Egypt: Magma genesis and generation of continental crust in intra-oceanic arcs. *Lithos*, 132-133, 1–20.

Mazhari, S. A., Bea, F., Amini, S., Ghalamghash, J., Molina, J. F., Montero, M. P., & et al. (2009). The Eocene bimodal Piranshahr massif of the Sanandaj-Sirjan Zone, NW Iran: a marker of the end of the collision in the Zagros orogen. *Journal of the Geological Society*, 166, 53–69.

McDonough, W. F., & Sun, S. S. (1995). Composition of the Earth. *Chemical Geology*, 120, 223–253.

McDonough, W. F., Sun, S., Ringwood, A. F., Jagoutz, E., & Hofmann, A. W. (1992). Rb and Cs in the earth and moon and evolution of the earth's mantle. *Geochimica et Cosmochimica Acta*, 56, 1001–1012.

Mohajjel, M., Fergusson, C. L., & Sahandi, M. R. (2003). Cretaceous–Tertiary convergence and continental collision, Sanandaj-Sirjan Zone, Western Iran. *Journal of Asian Earth Sciences*, 21, 397–412.

Park, S. H., Lee, S. M., Kamenov, G. D., Kwon, S. T., & Lee, K. Y. (2010). Tracing the origin of subduction components beneath the South East rift in the Manus Basin, Papua New Guinea. *Chemical Geology* 269, 339–349.

Pearce, J. A. (1982). *Trace element characteristics of lavas from destructive plate boundaries*. In R. S. Thorpe (Ed.), Andesites (pp. 525–548).Wiley, Chichester.

Pearce, J. A. (1983). *The role of subcontinental lithosphere in the magma genesis at destructive plate margin*. In C. J. Hawkesworth, & M. J. Norry (Eds.), Continental Basalts and Mantle Xenoliths (pp. 230–249). Natwich Shiva.

Pearce, J. A., & Peate, D. W. (1995). Tectonic implications of the composition of volcanic arc magmas. *Annual Review of Earth and Planetary Sciences*, 23, 251–285.

Polat, A., & Hofmann, A. W. (2003). Alteration and geochemical patterns in the 3.7–3.8 Ga Isua greenstone belt, West Greenland. *Precambrian Research*, 126, 197–218.

Rajaieh, M., Khalili, M., & Richards, I. (2010). The significance of mafic microgranular enclaves in the petrogenesis of the Dehno Complex, Sanandaj–Sirjan belt, Iran. *Journal of Asian Earth Sciences*, 39, 24–36.

Sarkarinejad, K., Faghih, A., & Grasemann, B. (2008). Transpressional deformations within the Sanandaj-Sirjan metamorphic belt (Zagros Mountains, Iran). *Journal of Structural Geology*, 30, 818–826.

Schuth, S., Rohrbach, A., Münker, C., Ballhaus, C., Garbe-Schönberg, D., & Qopoto, C. (2004). Geochemical constraints on the petrogenesis of arc picrites and basalts, New Georgia Group, Solomon Islands. *Contributions to Mineralogy and Petrology*, 148, 288–304.

Shahbazi, H., Siebel, W., Pourmoafee, M., Ghorbani, M., Sepahi, A. A., Shang, C. K., & Vousoughi Abedini, M. (2010). Geochemistry and U–Pb zircon geochronology of the Alvand plutonic complex in Sanandaj–Sirjan Zone (Iran): New evidence for Jurassic magmatism. *Journal of Asian Earth Sciences*, 39, 668–683.

Shervais, J. W. (1982). Ti–V plots and the petrogenesis of modern and ophiolitic lavas. *Earth and Planetary Science Letters*, 59, 101–118.

Sun, S., & McDonough, W. F. (1989). *Chemical and isotopic systematics of oceanic basalts: implications for mantle composition and processes*. In A. D. Saunders, & Norry, M. J. (Eds.), Magmatism in the Ocean Basins (pp. 313–345). Geological Society (London), Special Publication, 42.

Tang, G., Wang, Q., Wyman, D. A., Li, Z. X., Zhao, Z. H., Jia, X. H., & et al. (2010). Ridge subduction and crustal growth in the Central Asian Orogenic Belt: Evidence from Late Carboniferous adakites and high-Mg diorites in the western Junggar region, northern Xinjiang (west China). *Chemical Geology*, 277, 281-300.

Taylor, S. R., & McLennan, S. M. (1985). *The Continental Crustal: Its Composition and Evolution*. Blackwell, Oxford.

Viruete, J. E., Díaz de Neira, A., Hernáiz Huerta, P. P., Monthel, J., García Senz, J., Joubert, M., & et al. (2006). Magmatic relationships and ages of Caribbean Island arc tholeiites, boninites and related felsic rocks, Dominican Republic. *Lithos*, 90, 161–186.

Viruete, J. E., Estaún, A. P., Weis, D., & Friedman, R. (2010). Geochemical characteristics of the Río Verde Complex, Central Hispaniola: Implications for the paleotectonic reconstruction of the Lower Cretaceous Caribbean island-arc. *Lithos*, 114, 168–185.

Wilkinson, J. F. G., & Le Maitre, R. W. (1987). Upper mantle amphiboles and micas and TiO_2, K_2O and P_2O_5 abundances and 100 Mg/(Mg + Fe^{2+}) ratios of common basalts and undepleted mantle compositions. *Journal of Petrology*, 28, 37–73.

Winchester, J. A, & Floyd, P. A. (1977). Geochemical discrimination of different magma series and their differentiation products using immobile elements. *Chemical Geology*, 20, 325–343.

Winchester, J. A., & Floyd, P. A. (1976). Geochemical magma type discrimination: application to altered and metamorphosed basic igneous rocks. *Earth and Planetary Science Letters*, 28, 459–469.

Woodhead, J. D., Eggins, S. M., & Johnson, R. W. (1998). Magma genesis in the New Britain island arc: further insights into melting and mass transfer processes. *Journal of Petrology*, 39, 1641–1668.

Yan Wang, C., Zhou, F. Z., & Qi, L. (2007). Permian flood basalts and mafic intrusions in the Jinping (SW China)–Song Da (northern Vietnam) district: Mantle sources, crustal contamination and sulfide segregation. *Chemical Geology*, 243, 317–343.

Yang, J. H., Chung, S. L., Wilde, S. A., Wu, F. Y., Chu, M. F., Lo, C. H., & et al. (2005). Petrogenesis of post-orogenicsyenites in the Sulu Orogenic Belt, East China geochronological, geochemical, and Nd–Sr isotopic evidence. *Chemical Geology*, 214, 99–125.

Zhang, X., Zhang, H., Tang, Y., Wilde, S. A., & Hu, Z. (2008). Geochemistry of Permian bimodal volcanic rocks from central Inner Mongolia, North China: Implication for tectonic setting and Phanerozoic continental growth in Central Asian Orogenic Belt. *Chemical Geology*, 249, 262–281.